

Article

# Electric Aerospace Actuator Manufactured by Laser Powder Bed Fusion

Borja Lizarribar <sup>1,2,\*</sup>, Borja Prieto <sup>1,2</sup>, Miren Aristizabal <sup>1,2</sup>, Jose Manuel Martín <sup>1,2</sup>, Miguel Martínez-Iturralde <sup>1,2</sup>, Ekain San José <sup>3</sup>, Ione Golvano <sup>3</sup> and Sergio Montes <sup>3</sup>

<sup>1</sup> CEIT-Basque Research and Technology Alliance (BRTA), Manuel Lardizabal 15, 20018 San Sebastián, Spain

<sup>2</sup> Universidad de Navarra, Tecnun School of Engineering, Manuel Lardizabal 13, 20018 San Sebastián, Spain

<sup>3</sup> Egile Mechanics S.L., Polígono Industrial Kurutz-Gain, 12, 20850 Mendaro, Spain

\* Correspondence: blizarribar@ceit.es

**Abstract:** Recent advances in manufacturing methods have accelerated the exploration of new materials and advantageous shapes that could not be produced by traditional methods. In this context, additive manufacturing is gaining strength among manufacturing methods for its versatility and freedom in the geometries that can be produced. Taking advantage of these possibilities, this research presents a case study involving an electric aerospace actuator manufactured using additive manufacturing. The main objectives of this research work are to assess the feasibility of additively manufacturing electric actuators and to evaluate potential gains in terms of weight, volume, power consumption and cost over conventional manufacturing technologies. To do so and in order to optimise the actuator design, a thorough material study is conducted in which three different magnetic materials are gas-atomised (silicon iron, permendur and supermalloy) and test samples of the most promising materials (silicon iron and permendur) are processed by laser powder bed fusion. The final actuator design is additively manufactured in permendur for the stator and rotor iron parts and in 316L stainless steel for the housing. The electric actuator prototype is tested, showing compliance with design requirements in terms of torque production, power consumption and heating. Finally, a design intended to be manufactured via traditional methods (i.e., punching and stacking for the stator laminations and machining for the housing) is presented and compared to the additively manufactured design. The comparison shows that additive manufacturing is a viable alternative to traditional manufacturing for the application presented, as it highly reduces the weight of the actuator and facilitates the assembly, while the cost difference between the two designs is minimal.

**Keywords:** electric actuator; electric motor; permanent magnet; additive manufacturing; laser powder bed fusion; selective laser melting; AM; PBF; LPBF; SLM; iron–cobalt alloys; permendur; FeCo



**Citation:** Lizarribar, B.; Prieto, B.; Aristizabal, M.; Martín, J.M.; Martínez-Iturralde, M.; San José, E.; Golvano, I.; Montes, S. Electric Aerospace Actuator Manufactured by Laser Powder Bed Fusion. *Aerospace* **2023**, *10*, 813. <https://doi.org/10.3390/aerospace10090813>

Academic Editor: Kyriakos I. Kourousis

Received: 20 July 2023

Revised: 11 September 2023

Accepted: 14 September 2023

Published: 17 September 2023



**Copyright:** © 2023 by the authors. Licensee MDPI, Basel, Switzerland. This article is an open access article distributed under the terms and conditions of the Creative Commons Attribution (CC BY) license (<https://creativecommons.org/licenses/by/4.0/>).

## 1. Introduction

The trends set by more electric aircraft (MEA) aim to reduce the number of pneumatic, mechanical and hydraulic systems and replace them with electrically powered actuators [1]. This goal of electrifying the aerospace sector is also supported by the Clean Sky 2 programme, which aims to be the main contributor to the Commission's Flightpath 2050 goals, set by ACARE. These objectives are:

- A 75% reduction in CO<sub>2</sub> emissions.
- A 90% reduction in NO<sub>x</sub> emissions.
- The perceived noise of flying aircraft reduced by 65%.
- Air vehicles designed and manufactured to be recyclable.

For this matter, reducing the weight of aircraft components is a key factor, as aircraft weight is one of the main contributors to fuel consumption and, hence, emissions. In this scenario, additive manufacturing (AM) is gaining strength due to the advantages it reports

in terms of geometric flexibility and material savings. More specifically, AM in the aerospace sector has become a viable solution for the production of various parts, ranging from small cabin brackets [2] and hinge brackets [3], to larger and more critical components such as turbopump stators [4] and a rocket nozzles [5]. Moreover, AM has been proven effective for the construction of various aerospace components [6] and it is regarded to bring benefits over traditional manufacturing in terms of weight, lead time reduction and cost for a number of components [7].

In addition to the flexibility of the geometries that can be produced, AM also allows a wide variety of materials to be processed. A comprehensive review of the metallic materials available for AM is provided in [8], in which various materials are surveyed, such as Ni-based, Fe-based, Cu-based, Al-based, Ti-based and so on. Examples of aerospace components produced by AM can be found in [2,3,9] (Ti-based alloys), in [10] (Cu-based alloys) and in [11] (Fe-based alloys).

Not only have mechanical parts for aeronautics been produced already via AM, but also magnetic [12,13] and thermal management [14–18] components have been manufactured as well. It is worth highlighting the case presented in [12], in which the rotor and the shaft of a direct current (DC) motor for an UAV aircraft are manufactured via selective laser sintering (SLS) in A6 steel. Copper and aluminum alloys have been additively manufactured as well, showing promising results for electrical machine design in terms of heat extraction and loss reduction at high-frequency operation [19–21]. Further examples of electrical machine components made using AM and unusual magnetic materials can be found in [22,23] (Fe-Al alloy), [24] (17-4PH stainless steel) and [25] (pure Fe). In this regard, despite the wide variety of materials that can be produced by AM, the use of additively produced soft magnetic materials is not widespread. Nevertheless, various attempts at additively processing said materials can be found in [26–30] (FeSi alloys), [31,32] (FeCo alloys) and [33] (FeNi), for instance.

In the context of aircraft electrification, emission and weight reduction and additive manufacturing, the present work presents a case study involving the AM of an electric actuator for an active inceptor system. The Smart Active Inceptor system, developed by Safran Electronics & Defense, consists of a joystick-type control interface that provides tactile feedback to pilots for a civil tiltrotor aircraft, following a fly-by-wire concept. The aim of the present work has been to analyse the feasibility of manufacturing electric actuators using a laser powder bed fusion (LPBF) technique (also known as selective laser melting, SLM) and to evaluate the gains in terms of weight, volume, power consumption and cost over conventional manufacturing technologies. For this purpose, gas-atomised soft magnetic metallic compositions have been analysed, powder bed fusion (PBF) process parameters have been optimised and an electric actuator prototype has been manufactured.

This article is structured as follows: first, the case study is presented and the requirements for the designed actuator are briefly summarised in Section 2. The materials considered for the application and their assessment are then discussed in Section 3. Two equivalent actuator designs, one intended to be manufactured additively and the other one in traditional terms, are described in Section 4 and are compared in terms of weight, volume and cost. A brief note on the fabrication and testing of an AM actuator prototype is given in Section 5, and finally, the conclusions of the present work and some considerations regarding future work are stated in Section 6.

## 2. Case Study

As stated in Section 1, the case study presented in this research work involves the design and manufacturing of an electric actuator (or motor) for an active inceptor system, shown in Figure 1. As illustrated, the main elements of the system involve a handle, a kinematic joint that connects the two-axis movement of the grip to two motors/actuators and a set of safety brakes and resolvers for controlling those. The torque produced by the electric motors is what allows the user to experience controlled force-feedback when

holding the sidestick. The performance requirements specified for each of the motor units are summarised in Table 1.

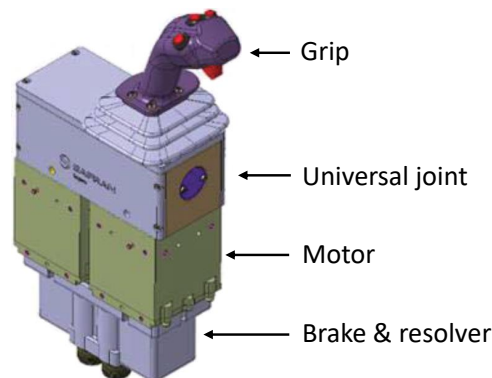


**Figure 1.** Smart Active Inceptor concept by Safran Electronics & Defense [34].

**Table 1.** Main requirements for the designed actuator.

Requirements	
Envelope	100 × 100 × 100 mm
Torque	8 N·m
Max. power consumption (stall conditions)	150 W
Max. temperature after 120 s operation (stall)	120 °C
Max. weight	3 kg

Regarding the AM approach for the actuator, the nearly zero speed of the inceptor application, which must provide force to the grip under no or little movement, makes it very suitable to consider the AM of the soft magnetic actuator parts. In conventional electric motors, which operate at non-zero frequencies (typically 50/60 Hz in industrial applications and 400 Hz in aircraft electrical power distribution), significant energy losses occur in the soft magnetic material parts due to induced eddy currents when subjected to variable magnetic fields. For this reason, it is common for stators and rotors in electrical machines manufactured by non-additive technologies to be made by die-cutting and stacking insulated thin silicon steel sheets (the addition of silicon increases the electrical resistivity of the material and reduces energy losses). For soft magnetic materials fabricated by AM, several techniques have been proposed to emulate the effect of lamination for reducing eddy current losses in the solid material [26,35,36].

In addition, the additive manufacturing of structural parts has also been considered in this project. The additive manufacturing of the hard magnetic parts has been discarded because, for the time being, except for very specific AM processes such as cold spray [37–39], the magnetic performance (coercivity, remanence) of the resulting magnets is far from that of conventional sintered rare earth magnets [40–43]. Additive manufacturing of copper coils has also not been considered due to the small size of the actuator and the high number of turns that the near-zero speed requires to achieve the desired voltage.

The result of the design exercise is shown in Section 4, after detailing the atomisation and optimisation of the additive manufacturing process.

### 3. Material Assessment and Testing

Additive manufacturing of stainless steels is well established in the literature [8] and metallic powder for the AM of different steel compositions is already available in the market. On the other hand, the commercial availability of magnetic alloys is much lower, so one of the main lines of research opened up by this project has been the AM of soft magnetic materials. Key highlights regarding gas atomisation of magnetic powders, LPBF processing

of said materials and heat treatment (HT) optimisation for permendur test samples are provided within this section.

### 3.1. Gas Atomisation of Soft Magnetic Materials

Gas atomisation is one of the main methods to manufacture the metallic powders used by the powder metallurgy industry [44]. It is highly versatile, as it can be used with many different alloys, the control of the particle size distribution is good and the output is high. Moreover, the powder has a low oxygen content and a spherical particle shape. These features make gas atomisation the reference technology for producing powders for AM. As illustrated by Figure 2, the principle of this powder production method is to transfer kinetic energy from a high-speed gas jet to a liquid metal stream that becomes unstable. The expansion of the gas around the molten stream causes a dramatic depressurisation and the disintegration of the liquid into small droplets which solidify as powder particles. In this work, experimental atomisations have been conducted in an atomisation unit (PSI model HERMIGA 75/3VI) using a close-coupled, convergent–divergent atomiser in which the gas nozzle has the shape of an annular slot (see Figure 2). The raw materials are charged into a high purity alumina crucible and melted by induction under argon. The atomisation chamber is also evacuated and purged with argon to minimise oxidation. The plant is capable of producing about 3 kg of powder per batch. The melt is superheated to 200 °C above its liquidus temperature, injected into the atomisation chamber and atomised using an argon stream at a stagnation pressure of 5.0–5.5 MPa.

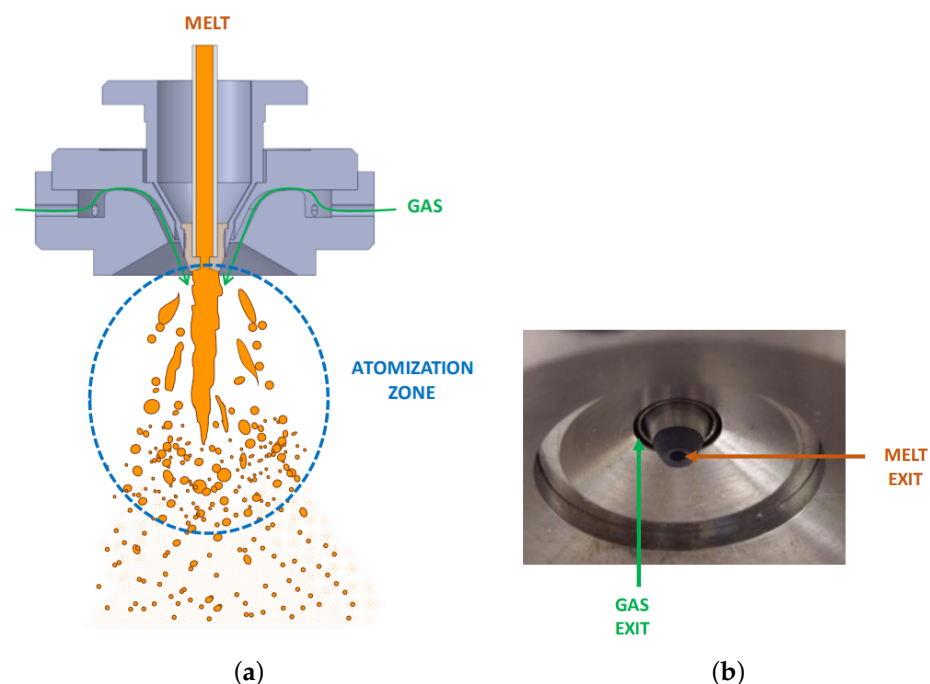


**Figure 2.** (a) Schematic diagram of the primary atomisation of a melt stream by the rapidly expanding gas; (b) photograph showing the proximity between the gas and the melt exits [45] (reproduced with permission from the authors).

Regarding the selection of soft magnetic materials for the magnetic circuit of electric actuators, the most relevant properties are high permeability, high saturation flux density and low coercivity. Three different soft magnetic material compositions that trade these properties have been considered thus within this project:

- Supermalloy: An 80% nickel–iron–molybdenum alloy with extremely high initial and maximum permeability and minimum hysteresis loss. It is used primarily for transformer cores, tape-wound toroids, electromagnetic shielding and laminations

operating at very low magnetic field strengths. Supermalloy has been manufactured via LPBF/SLM, for instance, in [46].

- Fe6.5Si: A soft magnetic alloy with high magnetic permeability, low coercive force and low iron loss. The main advantage of this material is that it has the lowest price among the options analysed. Additionally, this material has also presented promising results in terms of magnetic properties [47,48].
- Permendur (49Fe49Co2V): A cobalt–iron soft-magnetic alloy that stands out for its high magnetic saturation. Due to its high price, it is used in high-end applications, such as aerospace actuators, tape toroids and medium-frequency transformer laminations. Examples of LPBF processing of permendur can be found in [49].

Within this project, Fe6.5Si powder was purchased from Sandvik Osprey Ltd.(Sandviken, Sweden), in the 15–45  $\mu\text{m}$  fraction, and supermalloy and permendur compositions were gas-atomised and then sieved to the appropriate fraction at CEIT's premises. The magnetic properties of the powders at room temperature (around 22 °C) were evaluated from the hysteresis loop obtained in a Quantum Design PPMS-9T system with vibrating sample magnetometer (VSM). The magnetic characterisation of the powder is summarised in Figure 3 and Table 2. It can be observed that, as expected, supermalloy powder shows much lower magnetisation and coercivity figures. On the other hand, Fe6.5Si and permendur powder exhibit higher saturation flux density values, at the expense of a higher coercivity, which implies higher hysteresis losses.

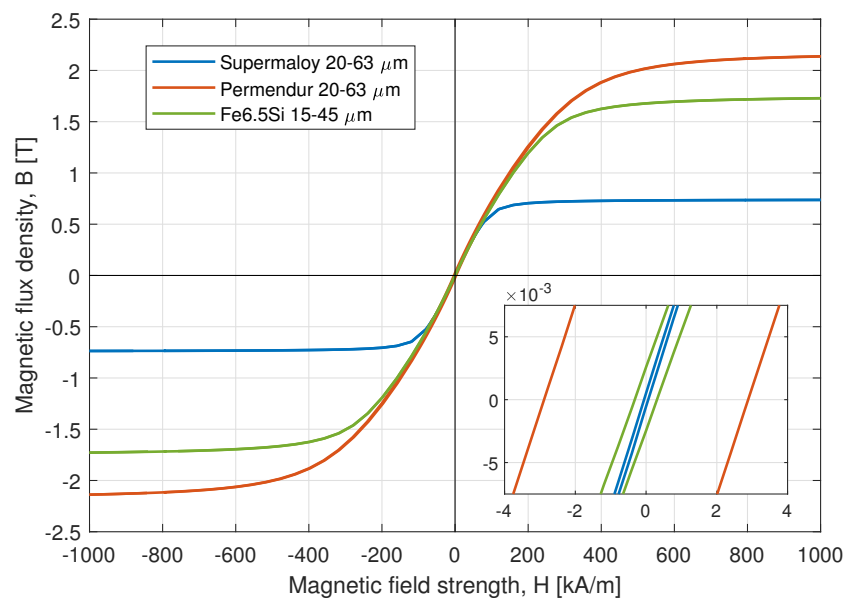


**Figure 3.** Magnetisation curves for the characterised powder at room temperature.

**Table 2.** Magnetic properties of the gas-atomised soft magnetic powders at room temperature:  $B_s$ : induction saturation;  $H_c$ : coercivity;  $H_K$ : anisotropy field.

Sample	$B_s$ (T)	$H_c$ (kA/m)	$H_K$ (kA/m)
Supermalloy 20–65 $\mu\text{m}$	0.746	0.061	103.5
Fe6.5Si 15–45 $\mu\text{m}$	1.767	0.313	273.7
Permendur 20–63 $\mu\text{m}$	2.178	2.928	330.2

Four different physical properties were measured for the magnetic powders: the flow rate, the apparent density, the tap density and pycnometer density. The flow rate quantifies the ability of each powder to flow, whereas the density of the powder allows one to estimate the internal porosity of the powders. The Hall flowmeter funnel method was used to

measure the flow rate and the apparent density of the powders, following Metal Powder Industries Federation (MPIF) standard #4 and #28, and an AccuPyc1330 pycnometer was used for the pycnometer density. MPIF standard #46 was followed to measure the tap density of the powders. Additionally, the chemical composition, morphology and microstructure of the powders were analysed via inductive coupled plasma mass spectrometry (ICP-OES, equipment: Varian 725-ES) and scanning electron microscopy (SEM). Finally, interstitial elements within the powder were measured by means of LECO analyses. A LECO TC-400 series oxygen/nitrogen fusion analyser was used to determine the oxygen and nitrogen content of and a LECO CS-200 Series carbon/sulphur combustion analyser was employed for the carbon and sulphur contents. The main physical properties are collected in Table 3. The Hausner ratio, obtained as the ratio of the tap to apparent density, gives information about the flowability of the powder material; with a Hausner ratio greater than 1.25 being an indication of poor flowability for AM processes. As observed in the table, the three metallic compositions exhibit a suitable Hausner ratio for PBF applications.

**Table 3.** Physical properties of the gas-atomised soft magnetic powders.

Sample	Flow Rate (s/50 g)	Apparent Density (g/cm <sup>3</sup> )	Tap Density (g/cm <sup>3</sup> )	Pycnometer Density (g/cm <sup>3</sup> )	Hausner Ratio
Superalloy	No flow	4.45	5.33	8.6	1.20
Fe6.5Si	19.7	3.89	4.54	7.4	1.17
Permendur	No flow	4.45	5.19	8.1	1.16

Due to the requirements of the application (i.e., very high torque density and near-zero speed), it was decided to discard the supermalloy for further analysis, as its low saturation flux density impacts negatively on the weight reduction capability for the actuator and the magnetic losses are of little importance due to the very low frequency of operation.

### 3.2. Laser Powder Bed Fusion of Test Samples

After analysing the gas-atomised powder, testable parts were produced in a Renishaw AM 400 machine. The size of the manufactured test samples is 5 × 10 × 48 mm, adequate both for mechanical and magnetic characterisation tests. The test samples were mechanically characterised in a universal testing machine (Instron 5892), whereas the DC magnetic hysteresis loop for the samples was measured using an adjustable pole electromagnet (GMW magnet systems 3470). For both AM-processed materials, Fe6.5Si and permendur, an optimisation of the LPBF process parameters, namely hatch distance, laser power and scan speed, was carried out to obtain the best combination in terms of cracks, porosity and productivity. The search for optimal process parameters was conducted through several iterations under a design of experiments (DoE) approach.

- **Fe6.5Si test samples**

In the LPBF parameter development process for the Fe6.5Si alloy, four iterations were performed. Test samples manufactured during the first three iterations presented either burnt surfaces, cracks or micro-cracks. In the fourth and final iteration, test samples with no cracks and an acceptable porosity level of 1.3% were attained. The parameter optimisation process for the Fe6.5Si is illustrated in Figure 4.

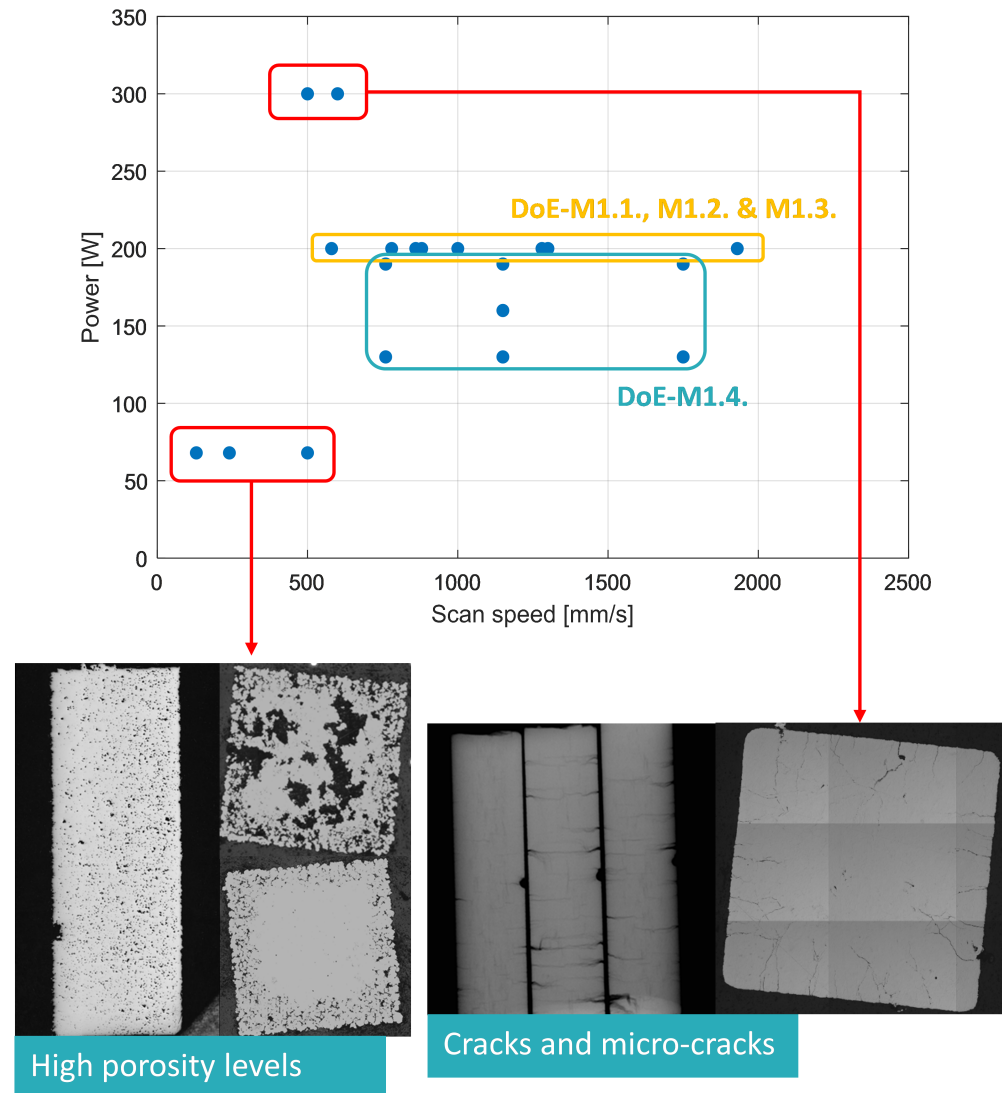


**Figure 4.** LPBF parameter development process for the Fe6.5Si alloy.

Magnetic measurements on the test samples manufactured in the last DoE iteration showed average magnetisation saturation and coercivity values of 171 emu/g and 2.2 Oe, respectively; values which are not far from those obtained in the characterisation of the gas-atomised powders (see Table 2). However, despite the good magnetic properties demonstrated by the Fe6.5Si PBF specimens, all AM test samples showed an excessive brittleness and broke when machined to standardised mechanical test sample dimensions. This is due to the use of low energy densities and the tendency towards brittleness in as-built materials when using LPBF technology. At low deposition energies to avoid cracking of the samples (below 50 J/mm<sup>3</sup>), there is a lack of fusion, resulting in a very porous component. Increasing the energy to densify the material eliminates porosity but introduces higher residual stresses due to higher temperature gradients.

- **Permendur test samples**

Two iterations were conducted during the PBF process optimisation for permendur. The AM test samples manufactured for the best parameter set show promising results, achieving densities greater than 99% in all directions and with no presence of cracks or microcracks. The PBF process optimisation is represented in Figure 5.

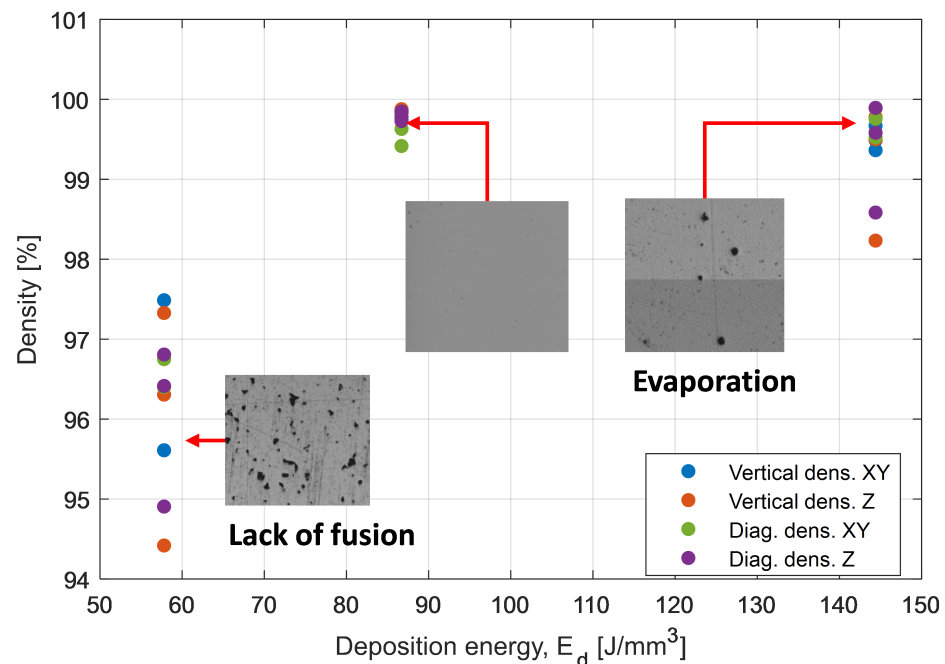


**Figure 5.** LPBF parameter development process for the permendur alloy.

Due to the good results obtained for permendur and the brittleness of the AM Fe6.5Si test samples, it was decided in the project to discard the latter and further continue the research with the permendur alloy.

### 3.3. Heat Treatment Optimisation for Permendur Test Samples

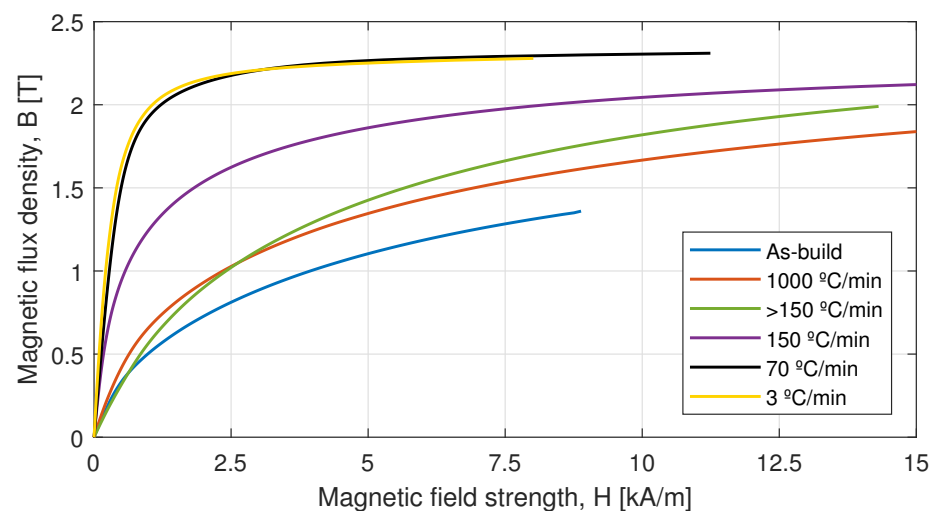
This sub-section deals with the selection of the most favourable heat treatment for LPBF-processed permendur. Preliminary measurements on the AM permendur test samples confirmed that, as the literature suggests, the as-built material has excellent mechanical properties (i.e., yield strength and elongation), but poor magnetic properties. On the other hand, the reference heat treatment for iron-cobalt alloys (heating in an inert atmosphere up to 870 °C for 4 h, followed by a slow cooling of 3 °C/min [50]) resulted in excellent magnetic properties, but brittle behaviour. As the actuator parts designed in permendur are intended to have both a magnetic and a structural function, significant efforts are required to achieve a heat treatment that satisfactorily balances the magnetic and mechanical properties of the material. Specifically, the focus was placed on the cooling rate after heating the samples.

A first trial demonstrated that the holding time for the heat treatment (i.e., 12 h versus 4 h at 855 °C in an argon atmosphere) has little influence on the mechanical and magnetic properties of the permendur test samples. On the contrary, the cooling rate has a huge influence. Five different cooling rates were analysed, ranging from 3–150 °C/min (slow-cooled in furnace), to >150 °C/min with forced air cooling and around 1000 °C/min with water quenching. The results obtained for the mechanical and magnetic properties are summarised in Table 4 and Figure 6, respectively.

**Table 4.** Mechanical properties for the permendur test samples according to the applied cooling rate.

Treatment	Cooling Rate [°C/min]	Ultimate Tensile Strength [MPa]	Yield Strength [MPa]	Elongation [%]
As-built	-	924	852	16.5
	1000 <sup>1</sup>	854	543	20.0
HT: 855 °C / Ar / 4 h	>150 <sup>2</sup>	645	296	10.0
	150 <sup>3</sup>	659	332	6.0
	70 <sup>3</sup>	449	302	3.6
	3 <sup>3</sup>	340	262	1.7

<sup>1</sup> Water-quenched; <sup>2</sup> air-cooled; <sup>3</sup> cooled inside furnace.

**Figure 6.** Mean magnetisation curve (1st quadrant) for the permendur test samples according to the applied cooling rate.

The variation of the magnetic and mechanical properties for permendur as a function of the cooling rate is explained by the eutectic diagram of the material, shown in Figure 7. With a composition of almost 50-50 between iron and cobalt, the significant phases for permendur are the  $\alpha$ , with a disordered body-centred cubic (BCC) structure, and the  $\alpha'$ , with an ordered CsCl-B2 type BCC structure. The  $\alpha$  phase has, in general terms, a very fine grain size, good mechanical properties and poor magnetic properties. The  $\alpha'$  phase, on the other hand, corresponds to a microstructure with large grains, poor mechanical properties and excellent magnetic properties.

The microstructures obtained by field emission gun scanning electron microscopy (FEG-SEM) for a number of the different applied cooling rates are shown in Figure 8. The microstructures present evident differences, with the as-built and fast-cooled (1000 °C/min) test samples exhibiting very fine grains and a disordered BCC structure, in accordance with the phase diagram. During the slow cooling (3 °C/min) process, the microstructure of the samples transforms to a fully  $\alpha'$  phase, showing larger grains. The test sample force cooled down with air at >150 °C/min presents a mix of ordered  $\alpha'$  and disordered  $\alpha$  phases, which leads to a compromise between magnetic and mechanical properties.

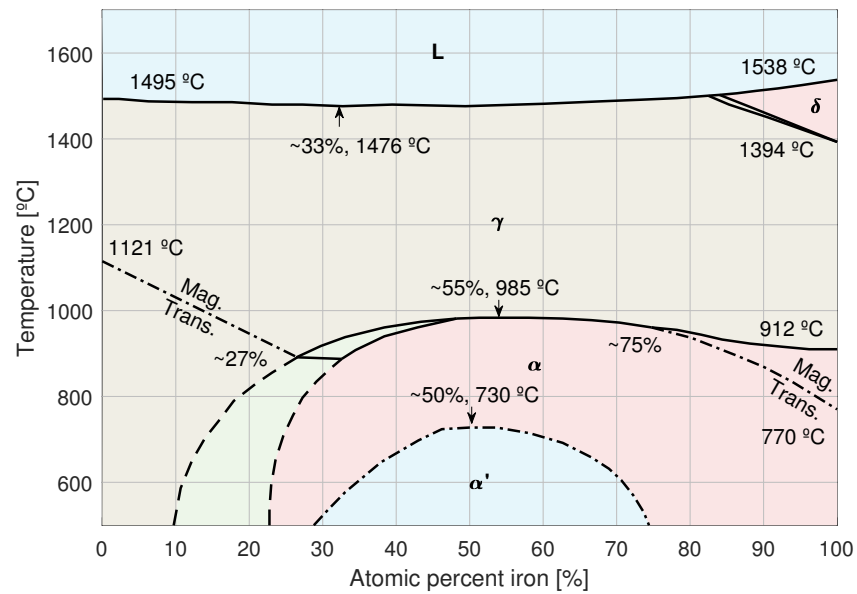


**Figure 7.** Phase diagram for permendur (redrawn from data from [51]).

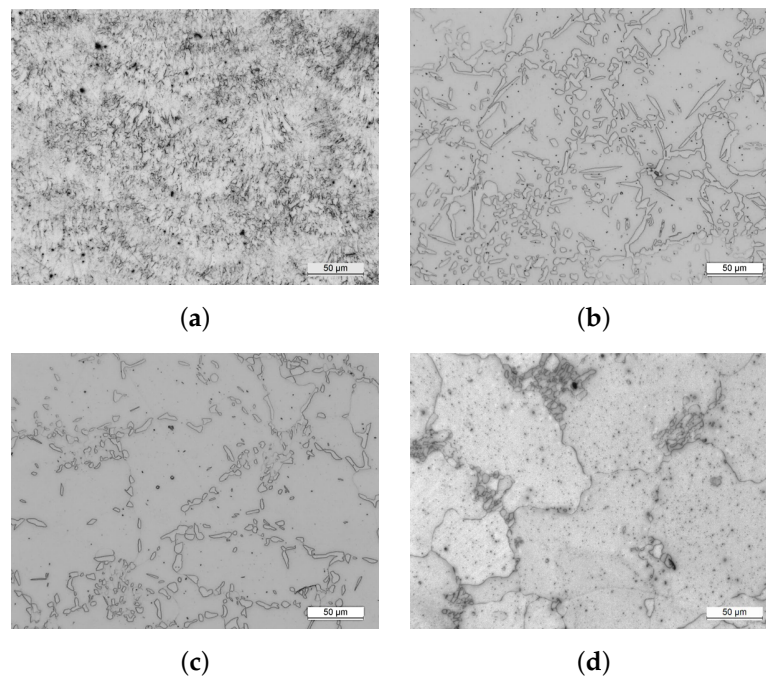


**Figure 8.** Microstructures exhibited by permendur test samples for different cooling rates after heat treatment: (a) as-built; (b) 1000 °C/min (water-quenched); (c) >150 °C/min (air-cooled); (d) 3 °C/min (cooled inside furnace).

In the present project, as a compromise between mechanical and magnetic properties, it was decided to continue with a cooling rate of 150 °C/min, so that the material allows for an elongation of at least 6% and the subsequent machining does not jeopardise the integrity of the additively manufactured parts.

#### 4. Electrical Actuator Designs

This section presents two designs of the case study involving the aerospace actuator: one that has been additively manufactured and the other that is intended to be manufactured using traditional production methods for comparison purposes.

##### 4.1. Additively Manufactured Actuator

The AM actuator design is presented in Figure 9. In this design, all parts are intended to be manufactured using LPBF, except for the rotor magnets, which are sintered; the stator coils; the bearings; and the cover, which is machined from aluminium as it has been considered that AM does not offer any advantages over conventional manufacturing for this part.

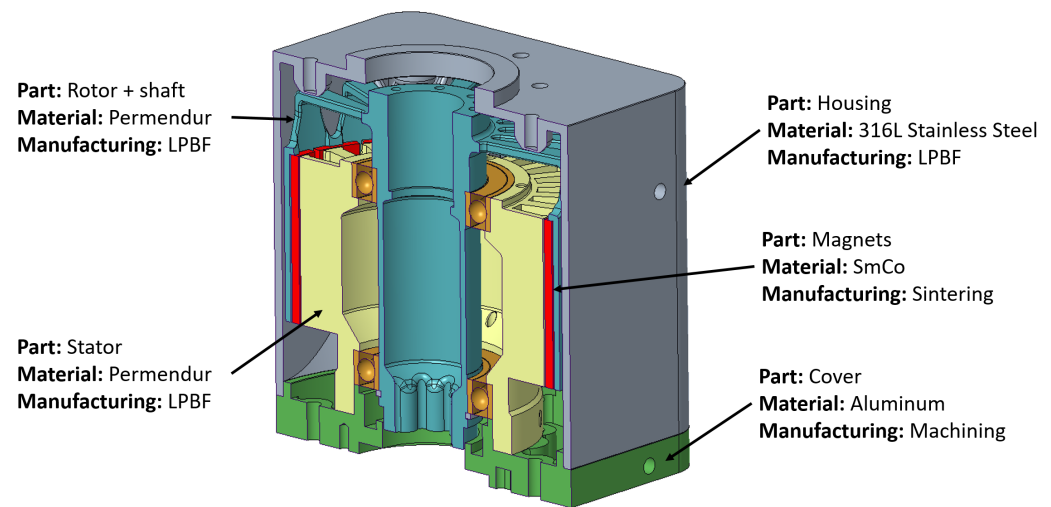


**Figure 9.** Additively manufactured actuator design.

One of the advantages of AM can be appreciated in the design of the rotor and stator parts, shown in blue and yellow, respectively. Both have been designed to have a dual function, magnetic and structural, leading to a significant reduction in the number of actuator parts should the materials have just a single function. The housing was designed in 316L stainless steel, as it has no magnetic function. The resulting assembly is quite simple with just four parts, excluding the magnets and the winding.

##### 4.2. Traditionally Manufactured Actuator

In order to have a fair comparison between additive and conventional methods, a detailed model design to be manufactured by traditional methods is presented next. Firstly, the machine was designed to meet the electromagnetic requirements. Conventional high-saturation flux density M800-50A electrical steel laminations were considered for the stator part, whereas for the rotor, a 410 stainless steel was contemplated due to its reasonable magnetic characteristics and its ability to have a dual magnetic-structural function. Should a non-ferromagnetic stainless steel have been selected for the shaft, the number of parts and joints in the assembly and the level of complexity would have increased significantly. To have equivalent designs with both manufacturing methods, the traditionally manufactured actuator was designed to have the same thermal behaviour as the additively manufactured one; that is, that similar winding temperatures are achieved when providing the rated 8 N·m torque for 120 s, as required by the application (see Table 1). The thermal behaviour for both actuator models was simulated via the lumped parameter thermal network software MotorCad 2023.2.1<sup>®</sup>. A comparison of the winding temperatures achieved in both models is provided in Figure 10.

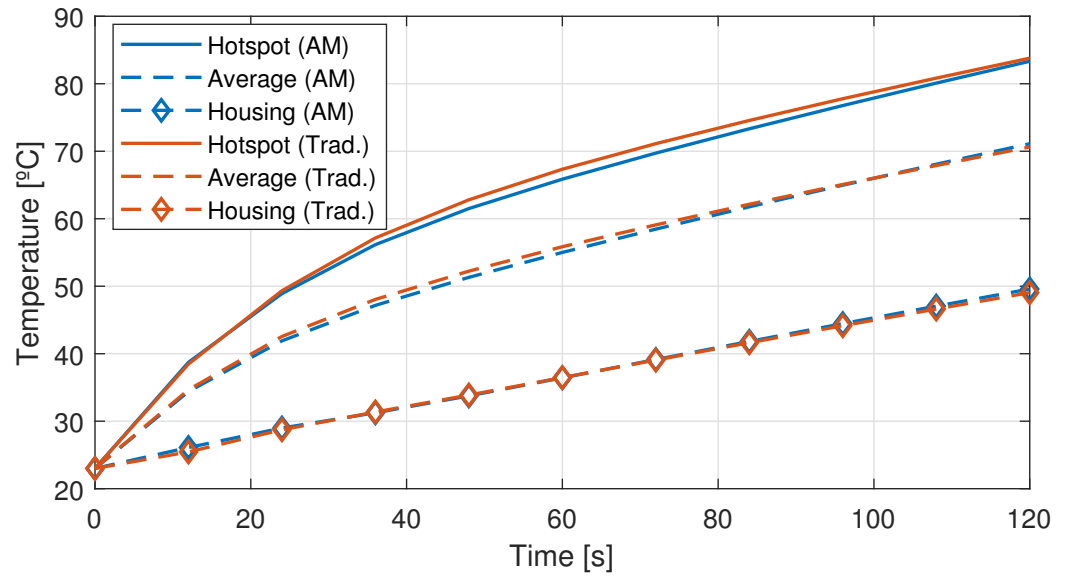


**Figure 10.** Winding temperatures in the AM (blue) and traditionally manufactured (red) actuator model estimated in MotorCad®.

The reduction in the cross-sectional area of the magnetic part of the stator due to the need to include an additional support part, the lower saturation flux density of the M800-50A electrical steel compared to the permendur and the poorer axial conductivity of the laminated part as opposed to the solid permendur have required a 25% increase in the axial length of the active parts, from 44 to 55 mm, to maintain the same thermal behaviour. The final mechanical design for the traditionally manufactured actuator is presented in Figure 11.

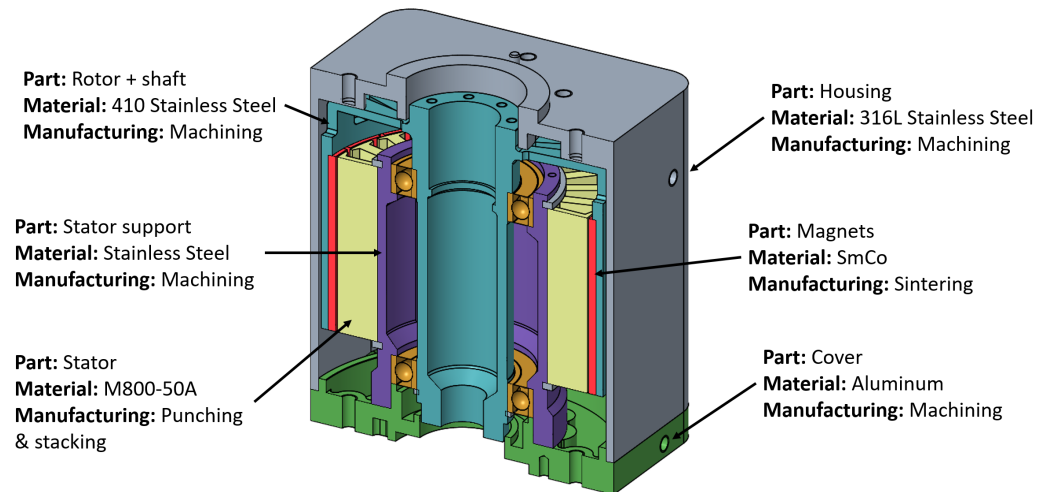


**Figure 11.** Traditionally manufactured actuator design.

#### 4.3. Comparative Study

The most noticeable difference between the two models is that the number of assembly parts is increased by one in the traditional design over the additively manufactured one. This aspect increases the difficulty of assembling and disassembling the actuator and reduces the reliability of the system. In addition and as mentioned above, the length of the active parts of the actuator design to be manufactured by conventional methods is 11 mm greater than that of the AM design. This implies an increase of 11% in volume and 23% in weight for the traditional concept over the AM one for the same thermal behaviour and power consumption. In fact, the actuator design intended for traditional manufacturing

does not meet the application requirements in terms of design envelope. The estimated weights for the various components of both designs are given in Table 5. Although neither design meets the desired target of 3 kg, the AM design comes very close to this figure.

**Table 5.** Weight comparison between the AM and conventionally manufactured actuator designs.

Part	LBPF	Traditional
<b>Stator</b>	0.82 kg	0.62 kg (lamination) 0.395 kg (support)
<b>Magnets</b>	0.22 kg	0.16 kg
<b>Endcap</b>	0.16 kg	0.16 kg
<b>Retaining rings</b>	0.00 kg	0.01 kg
<b>Ball bearings</b>	0.03 kg	0.03 kg
<b>Rotor</b>	0.56 kg	0.68 kg
<b>Casing</b>	1.11 kg	1.67 kg
<b>Winding</b>	0.36 kg	0.27 kg
<b>Total</b>	<b>3.26 kg</b>	<b>4.01 kg</b>

It is also of great interest to analyse the unitary manufacturing cost for both actuator models. The following cost analysis, presented in Table 6, is based on the assumption of having a production batch of several dozens of units per year for 10 years for both designs. Non-recurring costs have been excluded for the analysis, and due to the low number of units per year involved, a manual process instead of an automated one has been contemplated for the winding coils and magnet insertion. The costs considered in each case are the cost of materials, the cost of machine time, the machining or finishing required and the direct labour needed to assemble and complete each design. All costs are expressed as a percentage of the total manufacturing cost of a single unit of the additively manufactured actuator design.

To conclude, it is clear that the AM actuator design improves on the traditional model in terms of weight, volume and part count. Moreover, the estimated difference in cost per unit is not high, being the AM actuator design just 1.74% more expensive than the traditionally manufactured design.

The only advantage of the traditional actuator design is that there would be no torque reduction for a given current with increasing speed. While the designed actuator has a nearly zero operation speed, eddy-currents induced in the solid material at medium-to-high frequencies would make the AM design unsuitable for continuous high speed operation. A number of works in the relevant literature have tried to address the issue of iron losses in additively processed soft magnetic materials [26,35,36]. However, further advances are needed to achieve a similar performance to conventional laminated electrical steels for medium-to-high-frequency operation. Nevertheless, as this characteristic is not relevant for the application at hand as the actuator operates predominantly on standstill, the additively manufactured actuator design is regarded as superior.

**Table 6.** Cost analysis for the AM and traditionally manufactured actuator designs.

	Manufact. Method	Material	LPBF + HT	Punching and Stacking	Machining + HT	Labour	Subtotal
Rotor	AM	1.58%	22.16%	0.00%	4.92%	0.00%	28.66%
	Traditional	2.32%	0.00%	0.00%	19.51%	1.62%	23.45%
Stator	AM	1.51%	21.93%	0.00%	4.25%	0.00%	27.68%
	Traditional	0.18%	0.00%	7.57%	0.36%	0.45%	8.57%
Stator support	AM	0.00%	0.00%	0.00%	0.00%	0.00%	0.00%
	Traditional	0.60%	0.00%	0.00%	16.66%	1.40%	18.66%
Housing	AM	0.25%	14.41%	0.00%	3.70%	0.00%	18.37%
	Traditional	2.70%	0.00%	0.00%	17.63%	1.51%	21.84%
Endcap	AM	0.02%	0.00%	0.00%	0.76%	0.00%	0.78%
	Traditional	0.02%	0.00%	0.00%	0.76%	0.00%	0.78%
Windings	AM	0.51%	0.00%	0.00%	0.00%	7.71%	8.22%
	Traditional	0.38%	0.00%	0.00%	0.00%	8.08%	8.46%
Magnets	AM	1.00%	0.00%	0.00%	0.00%	1.63%	2.63%
	Traditional	0.80%	0.00%	0.00%	0.00%	2.04%	2.83%
Integration and testing	AM	0.00%	0.00%	0.00%	0.00%	13.65%	13.65%
	Traditional	0.00%	0.00%	0.00%	0.00%	13.65%	13.65%
					Total	AM	100.00%
						Traditional	98.26%

## 5. Manufacturing and Testing

A prototype of the AM actuator design was manufactured by Egile Mechanics via LPBF/SLM in a Renishaw AM 400 machine. After the LPBF processing of the permendur parts and the application of the heat treatment, the stator and rotor parts were separated from the corresponding baseplate via electrical discharge machining (EDM) and were sandblasted. After checking of the surface homogeneity, required machining processes such as grinding and drilling were performed and a dimensional control was established, leading to satisfactory results. Regarding the housing of the actuator, it was additively manufactured using gas-atomised 316L stainless steel powder purchased to Oerlikon. A stress relieve heat treatment according to standard AMS 2759-4 [52] was applied to the housing and, after separating it from the support, it was milled and drilled and again, compliance with required dimensions was checked. The stator part was wound with copper coils and immersed in insulating impregnation, SmCo magnets were glued to the rotor and the actuator cover was machined from an aluminium block. Finally, the full actuator prototype was assembled. The additively manufactured parts and the process of assembling the prototype are shown in Figure 12. It can be appreciated in the figure that some magnets partially broke at the outer end when removing the tooling employed to facilitate their insertion. Although this is an issue to be avoided, subsequent tests have confirmed that this fact has led to no significant influence on the operation of the actuator, as will be discussed below.

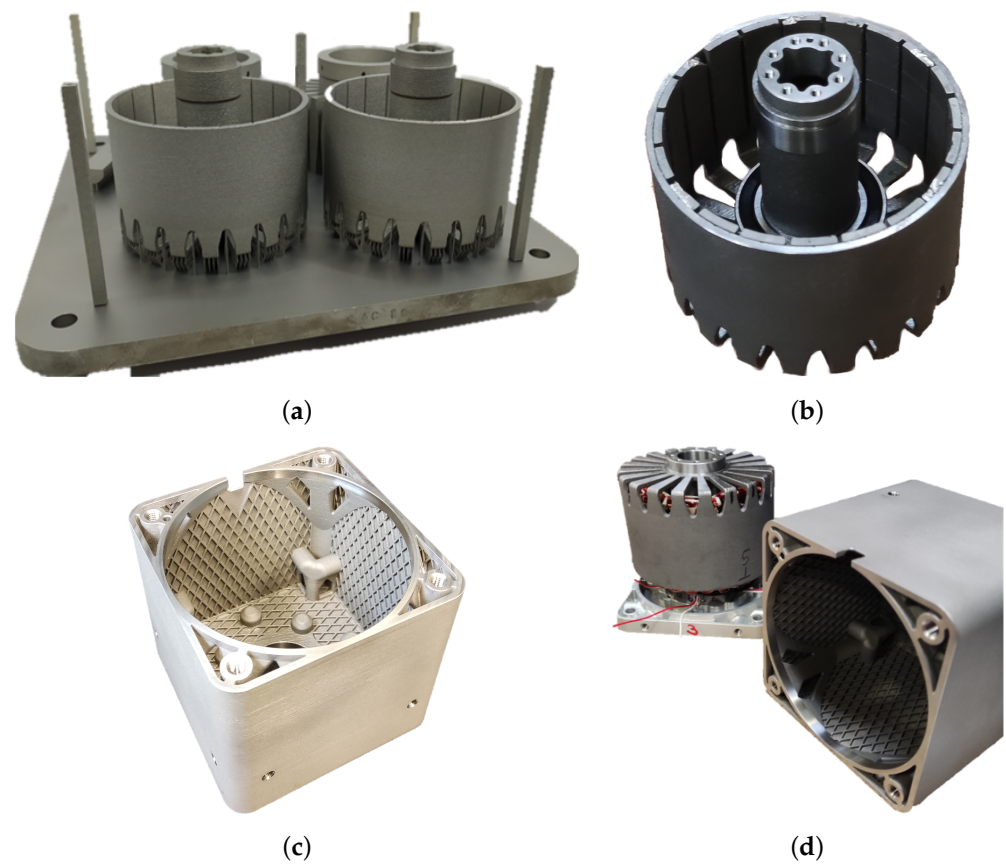


**Figure 12.** Prototype manufacturing: (a) as-built parts; (b) rotor and magnets; (c) casing; (d) assembling.

The actuator prototype was tested in a dedicated test set up designed to verify the application requirements. This test setup is illustrated in Figure 13. Additionally, current and voltage probes to measure the power consumed by each motor phase and Pt100 temperature sensors to monitor the winding temperatures during operation were employed.

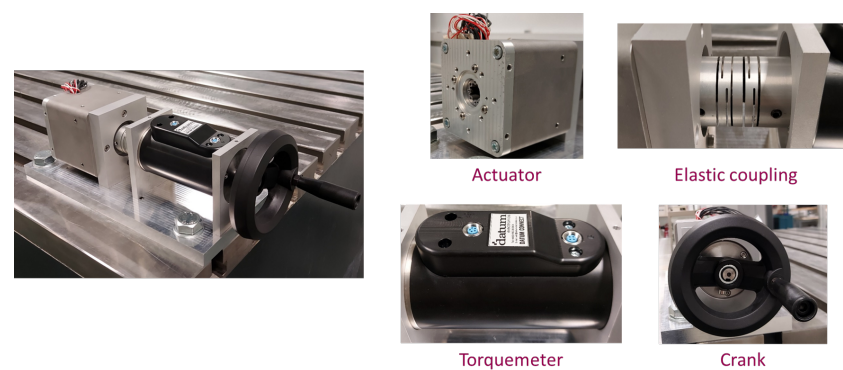


**Figure 13.** Test bench configuration.

To verify the torque capability of the actuator, the rated current of  $10 A_{RMS}$  was supplied to the motor phases at standstill ( $\sqrt{2} \times 10 = 14.2 A$  for phase A and  $-7.1 A$  for phases B and C) via a programmable switch mode DC power supply (Amrel SPS250-40). The actuator was slowly rotated by driving the crank and the readings of the torquemeter were recorded. The maximum registered value, which corresponds to the actual torque capability of the actuator for the rated current, is  $8.00 N\cdot m$ , which perfectly matches the design value for the actuator.

Finally, a standstill temperature test was carried out. The rated current was applied for 120 s and the temperatures in the actuator end-windings were recorded every 1 s. The results from the DC heating test are shown in Figure 14. The temperature rise for the hottest spot in the actuator is 60.4 °C, with a maximum temperature of 90.4 °C, whereas the temperature rise predicted in MotorCad® during the design stage is of 60.8 °C, showing good agreement between the simulation models and the experimental prototype. In both cases, the maximum temperature in the actuator is well below the established maximum of 120 °C (see Table 1). During the heating test, the DC power consumption was measured as well by monitoring the current and voltage drop across each phase. The DC power consumption after the heating test is 145 W, which is 3.33% lower than the established limit of 150 W.

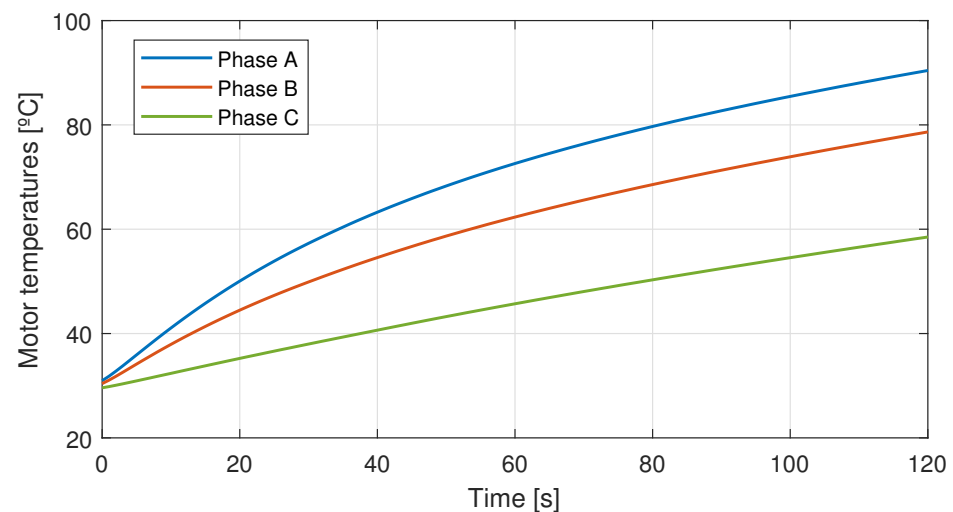


**Figure 14.** Temperatures in the stator end-windings registered during the standstill heating test on the actuator.

On completion of the performance tests on the LPBF actuator, the main requirements defined in Table 1 are considered to be fulfilled. Although the weight requisite was not satisfied, it should be noted that this requirement was considered to be very demanding from the start of the project. Nevertheless, the additively manufactured design involves a significant weight improvement over the design intended to be manufactured traditionally and over the preexisting LATM design.

## 6. Conclusions

This article presents the material assessment and the design of an electric aerospace actuator manufactured additively via laser powder bed fusion. Three different soft magnetic material compositions were investigated, with permendur (49Fe49Co2V) being selected as the most suitable material for the defined application. After optimising the powder bed fusion process parameters and the heat treatment that balances the mechanical and magnetic properties of the material, the designed actuator was manufactured and tested, showing good agreement between the experimental and design values and fulfilling the main design requirements. Additionally, a comparison with an actuator design intended to be manufactured via conventional means was provided. From the comparative study, it can be concluded that AM is a competitive manufacturing method for the application at hand, as the AM design improves on the traditional design in terms of weight, volume and part number, while the manufacturing cost for series production is just 1.74% higher according to a detailed cost analysis, maintaining the same performance characteristics.

The present work demonstrates that additive manufacturing can be an attractive technology for manufacturing low-frequency magnetic components (e.g., actuators, rotors) and for achieving multifunctional parts that simplify the integration and assembly of

components. However, for higher-frequency applications, the losses occurring in the non-laminated materials are an issue to be addressed, as shown in previous work on the matter [26,35,36].

A limitation of the work presented is that no tests have been carried out to determine the fatigue behaviour and reliability of the parts processed by LPBF. Therefore, future work on the subject should investigate this aspect, particularly with regard to mechanical vibration and ageing due to thermal cycling. Additional points worth researching include assessing different magnetic alloys (hard and soft), testing AM technologies other than LPBF for the manufacture of electrical machines and researching into the AM of conductors.

**Author Contributions:** Conceptualisation, B.L., B.P. and M.A.; methodology, B.L., B.P., M.A., J.M.M., M.M.-I., E.S.J., I.G. and S.M.; software, B.L. and B.P.; validation, B.L., M.A. and I.G.; original draft preparation B.L., B.P., M.A., J.M.M., I.G. and S.M.; review and editing, M.M.-I. and E.S.J.; project administration, M.M.-I. and E.S.J.; funding acquisition, M.M.-I., B.P., M.A., J.M.M., E.S.J. and I.G. All authors have read and agreed to the published version of the manuscript.

**Funding:** This research was funded by the European Union’s Clean Sky 2 Joint Undertaking programme under topic JTI-CS2-2018-CfP09-SYS-02-56 and grant agreement ID 865206.

**Data Availability Statement:** The data presented in this study are available on request from the corresponding author. The data are not publicly available for confidentiality reasons.

**Acknowledgments:** The authors are grateful to Safran Electronics & Defense as Topic Manager of the corresponding Clean Sky 2 project and to Lancor 2000 S.Coop for their help in manufacturing the actuator prototype.

**Conflicts of Interest:** The authors declare no conflicts of interest.

## Abbreviations

The following abbreviations are used in this manuscript:

AM	Additive Manufacturing
BCC	Body-Centred Cubic
DC	Direct Current
DoE	Design of Experiments
EDM	Electrical Discharge Machining
FEG	Field Emission Gun
HT	Heat Treatment
ICP	Inductive Coupled Plasma
LPBF	Laser Powder Bed Fusion
MPIF	Metal Powder Industries Federation
OES	Optical Emission Spectrometry
PBF	Powder Bed Fusion
SEM	Scanning Electron Microscopy
SLM	Selective Laser Melting
SLS	Selective Laser Sintering
VSM	Vibrating Sample Magnetometer

## References

1. Mohamed, M.A.A.; Yeoh, S.S.; Atkin, J.; Hussaini, H.; Bozhko, S. Efficiency Focused Energy Management Strategy Based on Optimal Droop Gain Design for More Electric Aircraft. *IEEE Trans. Transp. Electrif.* **2022**, *8*, 4205–4218. [CrossRef]
2. Orme, M.E.; Gschweidl, M.; Ferrari, M.; Vernon, R.; Madera, I.J.; Yancey, R.; Mouriaux, F. Additive Manufacturing of Lightweight, Optimized, Metallic Components Suitable for Space Flight. *J. Spacecr. Rocket.* **2017**, *54*, 1050–1059. [CrossRef]
3. Meng, L.; Zhang, W.; Quan, D.; Shi, G.; Tang, L.; Hou, Y.; Breikopf, P.; Zhu, J.; Gao, T. From Topology Optimization Design to Additive Manufacturing: Today’s Success and Tomorrow’s Roadmap. *Arch. Comput. Methods Eng.* **2020**, *27*, 805–830. [CrossRef]
4. Paul, G.; Omar, M.; Nathan, A. Intro to additive manufacturing for propulsion systems. In Proceedings of the AIAA Joint Propulsion Conference, Cincinnati, OH, USA, 9–11 July 2018; p. 83.
5. Steffen, D. Case Study: Additive Manufacturing. 3D Printing a Rocket Engine. Available online: <https://www.etmm-online.com/3d-printing-a-rocket-engine-a-886960/> (accessed on 10 February 2023).

6. Werkheiser, N. Overview of NASA Initiatives in 3D Printing and Additive Manufacturing. In Proceedings of the 2014 DoD Maintenance Symposium, Birmingham, AL, USA, 17–20 November 2014.
7. Barroqueiro, B.; Andrade-Campos, A.; Valente, R.A.F.; Neto, V. Metal Additive Manufacturing Cycle in Aerospace Industry: A Comprehensive Review. *J. Manuf. Mater. Process.* **2019**, *3*, 52. [CrossRef]
8. Blakey-Milner, B.; Gradl, P.; Snedden, G.; Brooks, M.; Pitot, J.; Lopez, E.; Leary, M.; Berto, F.; du Plessis, A. Metal additive manufacturing in aerospace: A review. *Mater. Des.* **2021**, *209*, 110008. [CrossRef]
9. Chen, W.; Li, Z. *Additive Manufacturing of Titanium Aluminides*; Elsevier: Amsterdam, The Netherlands, 2019; pp. 235–263. [CrossRef]
10. Woolley, S. Hot Stuff: To Build More Affordable Rocket Engines, NASA Researchers Are Using the Latest 3D Printers — And 1 Ancient Metal. Available online: <https://www.ge.com/news/reports/hot-stuff-to-build-more-affordable-rocket-engines-nasa-researchers-are-using-the-latest-3d-printers-and-1-ancient-metal> (accessed on 10 February 2023).
11. 3D Print, NASA Advances New Alloys and Scale of Metal Additive Manufacturing. Available online: <https://3dprint.com/278670/nasa-advances-new-alloys-and-scale-of-metal-additive-manufacturing/> (accessed on 10 February 2023).
12. Zaharia, S.M.; Pop, M.A.; Buican, G.R.; Chicos, L.A.; Stamate, V.M.; Pascariu, I.S.; Lancea, C. Design and Testing of Brushless DC Motor Components of A6 Steel Additively Manufactured by Selective Laser Sintering. *Aerospace* **2023**, *10*, 60. [CrossRef]
13. Wu, F.; EL-Refaie, A.M.; Al-Qarni, A. Minimization of Winding AC Losses Using Inhomogeneous Electrical Conductivity Enabled by Additive Manufacturing. *IEEE Trans. Ind. Appl.* **2022**, *58*, 3447–3458. [CrossRef]
14. Wrobel, R.; Hussein, A. A Feasibility Study of Additively Manufactured Heat Guides for Enhanced Heat Transfer in Electrical Machines. *IEEE Trans. Ind. Appl.* **2020**, *56*, 205–215. [CrossRef]
15. Kaur, I.; Singh, P. State-of-the-art in heat exchanger additive manufacturing. *Int. J. Heat Mass Transf.* **2021**, *178*, 121600. [CrossRef]
16. Robinson, A.; Colenbrander, J.; Deaville, T.; Durfee, J.; Kempers, R. A wicked heat pipe fabricated using metal additive manufacturing. *Int. J. Thermofluids* **2021**, *12*, 100117. [CrossRef]
17. Wu, F.; EL-Refaie, A.M.; Al-Qarni, A. Additively Manufactured Hollow Conductors for High Specific Power Electrical Machines: Aluminum vs Copper. In Proceedings of the 2021 IEEE Energy Conversion Congress and Exposition (ECCE), Vancouver, BC, Canada, 10–14 October 2021; pp. 4397–4404. [CrossRef]
18. Wu, F.; EL-Refaie, A.M.; Al-Qarni, A. Additively Manufactured Hollow Conductors Integrated With Heat Pipes: Design Tradeoffs and Hardware Demonstration. *IEEE Trans. Ind. Appl.* **2021**, *57*, 3632–3642. [CrossRef]
19. Selema, A.; Ibrahim, M.N.; Sergeant, P. Additively-Manufactured Ultra-Light Shaped-Profile Windings for HF Electrical Machines and Weight-Sensitive Applications. *IEEE Trans. Transp. Electrification* **2022**, *8*, 4313–4324. [CrossRef]
20. Simpson, N.; North, D.J.; Collins, S.M.; Mellor, P.H. Additive Manufacturing of Shaped Profile Windings for Minimal AC Loss in Electrical Machines. *IEEE Trans. Ind. Appl.* **2020**, *56*, 2510–2519. [CrossRef]
21. Selema, A.; Ibrahim, M.N.; Sergeant, P. Development of Novel Semi-Stranded Windings for High Speed Electrical Machines Enabled by Additive Manufacturing. *Appl. Sci.* **2023**, *13*, 1653. [CrossRef]
22. Hosek, M.; Krishnasamy, J.; Sah, S.; Bashaw, T. *Spray-Formed Hybrid-Field Electric Motor*; American Society of Mechanical Engineers, Charlotte, NC, USA, 21–24 August 2016. [CrossRef]
23. National Science Foundation, Catalyzing Commercialization: Spray-Formed Magnetic Composite Radically Improves Electric Motor Performance. Available online: <https://www.aiche.org/resources/publications/cep/2016/february/catalyzing-commercialization-spray-formed-magnetic-composite-radically-improves-electric-motor> (accessed on 10 February 2023).
24. Freeman, F.S.; Lincoln, A.; Sharp, J.; Lambourne, A.; Todd, I. Exploiting thermal strain to achieve an in-situ magnetically graded material. *Mater. Des.* **2019**, *161*, 14–21. [CrossRef]
25. Kresse, T.; Schurr, J.; Lanz, M.; Kunert, T.; Schmidt, M.; Parspour, N.; Schneider, G.; Goll, D. Additively Manufactured Transverse Flux Machine Components with Integrated Slits for Loss Reduction. *Metals* **2022**, *12*, 1875. [CrossRef]
26. Tiismus, H.; Kallaste, A.; Naseer, M.U.; Vaimann, T.; Rassolkin, A. Design and Performance of Laser Additively Manufactured Core Induction Motor. *IEEE Access* **2022**, *10*, 50137–50152. [CrossRef]
27. Garibaldi, M. Laser Additive Manufacturing of Soft Magnetic Cores for Rotating Electrical Machinery: Materials Development and Part Design. Ph.D. Thesis, University of Nottingham, Nottingham, UK, 2018.
28. Kallaste, A.; Vaimann, T.; Rassalkin, A. *Additive Design Possibilities of Electrical Machines*; IEEE: Piscataway Township, NJ, USA, 2018; pp. 1–5. [CrossRef]
29. Gargalis, L.; Madonna, V.; Giangrande, P.; Rocca, R.; Hardy, M.; Ashcroft, I.; Galea, M.; Hague, R. Additive Manufacturing and Testing of a Soft Magnetic Rotor for a Switched Reluctance Motor. *IEEE Access* **2020**, *8*, 206982–206991. [CrossRef]
30. Urbanek, S.; Frey, P.; Magerkohl, S.; Zimmer, D.; Tasche, L.; Schaper, M.; Ponick, B. *Design and Experimental Investigation of an Additively Manufactured PMSM Rotor*; IEEE: Piscataway Township, NJ, USA, 2021; pp. 1–6. [CrossRef]
31. Zhang, Z.Y.; Jhong, K.J.; Cheng, C.W.; Huang, P.W.; Tsai, M.C.; Lee, W.H. *Metal 3D Printing of Synchronous Reluctance Motor*; IEEE: Piscataway Township, NJ, USA, 2016; pp. 1125–1128. [CrossRef]
32. Tseng, G.M.; Jhong, K.J.; Tsai, M.C.; Huang, P.W.; Lee, W.H. Application of Additive Manufacturing for Low Torque Ripple of 6/4 Switched Reluctance Motor. In Proceedings of the 2016 19th International Conference on Electrical Machines and Systems (ICEMS), Chiba, Japan, 2 February 2017; pp. 1–4.

33. Metsä-Kortelainen, S.; Lindroos, T.; Savolainen, M.; Jokinen, A.; Revuelta, A.; Pasanen, A.; Ruusuvoori, K.; Pippuri, J. Manufacturing of topology optimized soft magnetic core through 3D printing. In *NAFEMS Exploring the Design Freedom of Additive Manufacturing through Simulation*; VTT Technical Research Centre of Finland Ltd.: Helsinki, Finland, 2016.
34. Clean Sky 2 Call for Proposals 09 (H2020-CS2-CFP09-2018-02), JTI-CS2-2018-CFP09-SYS-02-56: Additive Manufacturing Magnetic Motor. Available online: <https://www.cleansky.eu/calls> (accessed on 10 February 2023).
35. Plotkowski, A.; Pries, J.; List, F.; Nandwana, P.; Stump, B.; Carver, K.; Dehoff, R.R. Influence of scan pattern and geometry on the microstructure and soft-magnetic performance of additively manufactured Fe-Si. *Addit. Manuf.* **2019**, *29*, 100781. [[CrossRef](#)]
36. Tiismus, H.; Kallaste, A.; Belahcen, A.; Rassolkin, A.; Vaimann, T.; Ghahfarokhi, P.S. Additive Manufacturing and Performance of E-Type Transformer Core. *Energies* **2021**, *14*, 3278. [[CrossRef](#)]
37. Singh, S.; Payarou, T.; Bobby, M.; Lamarre, J.M.; Bernier, F.; Ibrahim, M.; Pillay, P. Cold Spray Additive Manufacturing of a Petal Shaped Surface Permanent Magnet Traction Motor. *IEEE Trans. Transp. Electrif.* **2023**. [[CrossRef](#)]
38. Lamarre, J.M.; Bernier, F. Permanent Magnets Produced by Cold Spray Additive Manufacturing for Electric Engines. *J. Therm. Spray Technol.* **2019**, *28*, 1709–1717. [[CrossRef](#)]
39. Bobby, M.; Singh, S.; Lamarre, J.M.; Ibrahim, M.; Bernier, F.; Pillay, P. In-Situ Magnetization of a Cold Sprayed Permanent Magnet Rotor Using an Impulse Magnetizer. In Proceedings of the IECON 2021—47th Annual Conference of the IEEE Industrial Electronics Society, Toronto, ON, Canada, 13–16 October 2021; pp. 1–6. [[CrossRef](#)]
40. White, E.M.H.; Kassen, A.G.; Simsek, E.; Tang, W.; Ott, R.T.; Anderson, I.E. Net Shape Processing of Alnico Magnets by Additive Manufacturing. *IEEE Trans. Magn.* **2017**, *53*, 1–6. [[CrossRef](#)]
41. Huang, J.; Yung, K.C.; Ang, D.T.C. Magnetic properties of SmCo5 alloy fabricated by laser sintering. *J. Mater. Sci. Mater. Electron.* **2019**, *30*, 11282–11290. [[CrossRef](#)]
42. Paranthaman, M.P.; Yildirim, V.; Lamichhane, T.N.; Begley, B.A.; Post, B.K.; Hassen, A.A.; Sales, B.C.; Gandha, K.; Nlebedim, I.C. Additive Manufacturing of Isotropic NdFeB PPS Bonded Permanent Magnets. *Materials* **2020**, *13*, 3319. [[CrossRef](#)] [[PubMed](#)]
43. Pigliaru, L.; Rinaldi, M.; Ciccacci, L.; Norman, A.; Rohr, T.; Ghidini, T.; Nanni, F. 3D printing of high performance polymer-bonded PEEK-NdFeB magnetic composite materials. *Funct. Compos. Mater.* **2020**, *1*, 4. [[CrossRef](#)]
44. Yule, A.; Dunkley, J. *Atomization of Melts: For Powder Production and Spray Deposition*; Oxford University Press: Oxford, UK, 1994.
45. Urionabarrenetxea, E.; Martín, J.M.; Avello, A.; Rivas, A. Simulation and validation of the gas flow in close-coupled gas atomisation process: Influence of the inlet gas pressure and the throat width of the supersonic gas nozzle. *Powder Technol.* **2022**, *407*, 117688. [[CrossRef](#)]
46. Firdosy, S.A.; Ury, N.E.; Witt, R.; Dillon, R.P.; Ravi, V.A. Laser-Deposited Soft Magnetic Fe–Ni–Mo Alloy: A Processing—Microstructure Study. *Metallogr. Microstruct. Anal.* **2022**, *11*, 108–118. [[CrossRef](#)]
47. Ouyang, G.; Chen, X.; Liang, Y.; Macziewski, C.; Cui, J. Review of Fe-6.5 wt%Si high silicon steel—A promising soft magnetic material for sub-kHz application. *J. Magn. Magn. Mater.* **2019**, *481*, 234–250. [[CrossRef](#)]
48. Zaied, M.; Ospina-Vargas, A.; Favergeon, J.; Fenineche, N. Additive Manufacturing of Soft Ferromagnetic Fe6.5%Si Annular Cores: Process Parameters and Magnetic Properties. *IEEE Trans. Magn.* **2022**, *58*, 1–9. [[CrossRef](#)]
49. Kurita, H.; Lohmuller, P.; Laheurte, P.; Nakajima, K.; Narita, F. Additive manufacturing and energy-harvesting performance of honeycomb-structured magnetostrictive Fe52–Co48 alloys. *Addit. Manuf.* **2022**, *54*, 102741. [[CrossRef](#)]
50. Carpenter Electrification: Hiperco<sup>®</sup> 50A, Specification for Heat Treatment. Original Document from Harris Semiconductor. 2020. Available online: <https://www.carpenterelectrification.com/hiperco-50a-datasheet50> (accessed on 22 May 2023).
51. Nishizawa, T.; Ishida, K. The Co-Fe (Cobalt-Iron) system. *Bull. Alloy. Phase Diagrams* **1984**, *5*, 250–259. [[CrossRef](#)]
52. AMS2759/4; Heat Treatment, Austenitic Corrosion-Resistant Steel Parts. SAE International: Warrendale, PA, USA, 2011. Available online: <https://www.sae.org/standards/content/ams2759/4/> (accessed on 19 July 2023).

**Disclaimer/Publisher's Note:** The statements, opinions and data contained in all publications are solely those of the individual author(s) and contributor(s) and not of MDPI and/or the editor(s). MDPI and/or the editor(s) disclaim responsibility for any injury to people or property resulting from any ideas, methods, instructions or products referred to in the content.